Structure and properties of the $Ni@Si_{12}$ cluster from all-electron *ab initio* calculations

Emmanuel N. Koukaras, Christos S. Garoufalis, and Aristides D. Zdetsis*
Department of Physics, University of Patras, 26500 Patras, Greece
(Received 19 December 2005; revised manuscript received 12 May 2006; published 20 June 2006)

The structural, electronic, and vibrational properties of the $Ni@Si_{12}$ cluster have been studied using all-electron *ab initio* calculations in the framework of the density functional theory (DFT) with the hybrid nonlocal exchange and correlation functional of Becke-Lee-Yang-Parr (B3LYP). Perturbation theory was also used for the lowest energy competing structures in order to unambiguously identify the ground state in view of marginal total energy differences at the DFT/B3LYP level of theory. To facilitate possible future experimental identification and to check the stability of the structures, we have performed vibrational analyses that include Raman and infrared spectra for the stable structures. Through the vibrational analysis, we have found that the C_{5v} symmetric Frank-Kasper structure, based on an icosahedral structural motif, which for some time was believed as the ground state, is unstable. Our calculations reveal a ground state of "cubic" D_{2d} symmetry, which at the fourth order of perturbation theory is about 1.3 eV lower than the alternative suggested ground state, based on a hexagonal structural motif. This distorted hexagonal structure of C_S symmetry at the DFT/B3LYP level of theory is practically isoenergetic to our cubic D_{2d} structure, with a marginal energy difference of about 0.04 eV. In addition to IR and Raman spectra, we have examined in detail electronic (bonding and binding), structural, and chemical characteristics that could be important for possible future applications of these or derived from these materials. Such characteristics include total and partial density of states, crystal orbital overlap populations, binding energies, ionization potentials, electron affinities, "chemical hardness," and embedding energies.

DOI: 10.1103/PhysRevB.73.235417 PACS number(s): 61.46.Bc, 36.20.Kd, 36.20.Ng, 36.40.Cg

INTRODUCTION

In the past 20 years there has been a considerable amount of research, both theoretical and experimental, on silicon based materials. The strong interest[1–5] on transition metal (TM) encapsulated Si clusters is due to the promising possible applications in nanotechnology and nanoelectronics, as well as to the understanding of fundamental properties. Recent developments in nanoelectronics have led to silicon based integrated circuits with elements as small as a few nanometers. Furthermore, stable silicon structures may serve as building blocks for the construction of nanoscale silicon based materials with a tunable band gap depending on the encapsulated transition metal atom (TMA).

The study of the physical and chemical properties at the interface between a metal and a silicon surface is very important.[6,7] Such study for small and medium size silicon clusters can reveal important information about the physical and chemical processes taking place at the metal-semiconductor interface. Knowledge and understanding of such processes could be very important, for instance, for the understanding and possible control of Schottky barrier heights. It has been speculated[8] that stable metal-containing silicon clusters may represent the earliest products formed at the interface.

Experimentally, the production and study of metal atom-silicon clusters was first reported by Beck.[8] In this work Beck observed the formation of metal-containing silicon clusters for three types of transition metals atoms, specifically tungsten (W), molybdenum (Mo), and chromium (Cr). The produced metal-containing silicon clusters exhibited increased stability compared to similar sized pure silicon clusters when subjected to photofragmentation. Hiura *et al.*[9] report that TMAs react with silane (SiH_4) producing Si clusters with an encapsulated TM atom. The endohedral TMA stabilizes the Si cage. The TMAs that react with silane to form stable cages have a partially filled *d* shell with two or more *d* electrons in the ground state. The $TM@Si_n$ clusters that are formed lose their reactivity to silane when *n* reaches 12, suggesting that $TM@Si_{12}$ complexes constitute stable clusters. Furthermore, Si_{12} has the added advantage that it can accommodate all relevant structural patterns—icosahedral, hexagonal, and cubic. Therefore, the study of its structural properties could prove very important for the design of larger TM-semiconductor systems.

From a theoretical point of view, the structural stability and electronic properties of $TM@Si_n$ clusters have been intensively investigated during the last few years with a large variety of theoretical methods. The results obtained by different techniques and/or different groups are not always compatible. This is more or less understandable in view of the complexity of the *ab initio* methods. The difficulties involved in such attempts can be readily appreciated when one considers that even for small pure Si clusters (which have been under investigation for many years) there are still numerous fundamental issues to be resolved.[10] The incorporation of TMAs, such as Ni, introduces partially filled *d* states (and possible different spin states), thus making the situation even more complex.

To date, little work has been done concerning specifically the $Ni@Si_{12}$ cluster. Menon *et al.*[11] have performed a series of tight-binding molecular dynamics (TBMD) as well as density functional theory (DFT) calculations in an effort to identify the energetically more stable isomer of $Ni@Si_{12}$. The results of both theoretical approximations suggest that the lowest energy Ni-encapsulated Si structure is a cage of

C_{5v} symmetry, such as the one shown in Fig. 1(h). Thus far, this conclusion has only been questioned by Singh *et al.*,[12] who has suggested that the structure of C_{5v} of Menon *et al.* is the third lowest in energy, while a distorted hexagonal prism and a chair structure are energetically more favorable than the former. Moreover, based on calculations on a double C_{5v} structure they claim that icosahedral packing is not favorable for Ni doping. Our work is a detailed study of the structural, electronic, and dynamical (vibrational) properties of possible $Ni@Si_{12}$ clusters. Our calculations indeed verify that the C_{5v} structure is not the ground state, and also reveal an energetically even lower structure as the equilibrium geometry of the $Ni@Si_{12}$ cluster. This conclusion is based on high (fourth) order perturbation theory. To facilitate possible future characterization, we have calculated a variety of properties including IR (infrared) and Raman vibrational spectra.

TECHNICAL DETAILS OF THE CALCULATIONS

We have performed all-electron *ab initio* calculations in real space in the framework of density functional theory within the generalized gradient approximation (GGA). For the lowest energy structures we have complemented our calculations with *ab initio* perturbation theory up to fourth order.

Several approaches have been adopted for the construction of the initial candidate geometries, since the usual geometry optimizations (performed at zero temperature) are more or less biased by the initial geometry and charge distribution. We started by considering structures based on ideal fcc and hcp cells, with up to second order neighbors from a central Ni atom, as well as additional structures based on hexagonal and icosahedral symmetry. In all of these cases we have performed symmetry unconstrained (C_1) geometry optimizations, in the framework of the density functional theory (DFT) using the gradient corrected BP86 functional[13] (GGA approximation). In these calculations we have used the SVP[14] basis set ($[4s3p1d]$ for Si and $[5s3p2d]$ for Ni) and the resolution of the identity[15] (RI) approximation for the two-electron integrals. In the second stage of the calculation we have symmetrized (wherever possible) the resulting structures (using loose symmetry criteria) and reoptimized them using tight optimization criteria, in the framework of the hybrid three parameter, nonlocal correlation functional of Becke-Lee-Yang-Parr (B3LYP).[16] Based upon prior experience,[17] the B3LYP functional gives very accurate results for both electronic and structural properties for Si. Moreover, for the case of silicon clusters,[10] it has been shown that the quality of B3LYP results is comparable to more sophisticated and computationally demanding methods, such as coupled-cluster with single, double, and perturbative triple excitations [CCSD(T)]. This second round of B3LYP calculations, performed under symmetry constraints, involves the larger triple-zeta quality split valence TZVP[18] basis set ($[5s4p1d]$ for Si and $[6s4p3d]$ for Ni). As a third and final step, all structures with non-C_1 symmetry were further checked for possible symmetry deviations by reoptimization without any symmetry constraints. The geometry optimizations were first performed with the TURBOMOLE program package,[19] using the Ahlrichs method[20] in redundant-internal-coordinate space, imposing convergence criteria for the residual force smaller than 10^{-4} atomic units. The second round of the (B3LYP/TZVP) optimizations was repeated with the GAUSSIAN-03[21] program package using the Berny algorithm[22] and (again) tight optimization criteria. These criteria, in addition to residual forces (both average and maximum) smaller than 1.5×10^{-5} a.u., involve also the condition of residual displacements (both average and maximum) smaller than 6×10^{-5} a.u. At this point, it should be noted that, even with tight optimization criteria, the optimization algorithms do not necessarily converge to stable solutions (geometries). For this reason, we have additionally performed a vibrational analysis in order to identify the structures which correspond to real minima of the calculated potential energy hypersurface.

We have checked that the correct ground state electronic configuration has been obtained by performing multiple calculations on different fixed spin states (singlet, triplet, etc.) and by employing an occupation number optimization procedure using (pseudo-Fermi) thermal smearing. In addition, the quality of the ground state wave functions was tested by suitable stability calculations. The vibrational calculations were also used to produce the IR and Raman spectra. Compared to infrared intensities (which depend on the square of the dipole moment gradients and the vibrational frequencies), the Raman activities involve the square of the polarizability derivative, which requires the calculation of the third derivative of the system energy with respect to coordinates and electric field. Thus, the calculation of Raman spectrum is by no means a trivial task. Needless to say, the same is true for the experimental measurements.[23] The IR and Raman experimental techniques for such systems are know as "surface plasmon-polariton enhanced Raman spectroscopy" and as "vacuum Fourier-transform infrared spectroscopy."[23] In the present work the polarizability derivatives were computed with the GAUSSIAN-03[21] program package, using numerical differentiation of the analytic dipole gradients with respect to the applied electric field. Static Raman intensities (zero-frequency, nonresonant) were computed in the double harmonic approximation,[23,24] ignoring cubic and higher force constants and omitting second and higher polarizability derivatives.

For the two energetically lowest structures, i.e., the D_{2d} and C_S isomers, which are almost isoenergetic at the B3LYP/TZVP level, we have also performed full Møller-Plesset[25] (MP) perturbation calculations up to fourth order (full MP4, or MP4SDTQ, i.e., MP4 involving single, double, triple, and quadruple excitations from the Hartree-Fock ground state Slater determinant) to test the conclusions obtained by the B3LYP method.

In order to make the electronic properties more transparent, we have developed a simple computer code to calculate crystal orbital overlap populations (COOP) as well as total and partial densities of states (DOS). The contribution of the Ni-related states to the total DOS is based on Mulliken population analysis (MPA), as is the calculation of the overlap populations. The overlap populations were used in order to produce the COOP diagrams. These diagrams, which were initially introduced by Hughbanks and Hoffmann,[26] are in

essence weighted DOS diagrams, the weights being the overlap population (OP_{AB}) of selected orbitals in the specific energy range. For the ith molecular orbital (MO), the overlap population between two groups (usually called fragments) A and B of atomic orbitals (AO) is given by

$$OP_{AB,i} = \sum_{a \in A} \sum_{b \in B} c_{ai}^{*} c_{bi} S_{ab},$$

where the index a runs on orbitals in group A and b runs on orbitals in group B. The coefficients c_{ai} represent the linear combination of atomic orbitals (LCAO) expansion of the ith MO on the AOs of group A, and S_{ab} is the overlap matrix. Interpretation of these diagrams is straightforward; regions of positive value correspond to bonding states while negative values correspond to antibonding states.

RESULTS AND DISCUSSION

Our B3LYP/TZVP calculations reveal two distinct, nearly isoenergetic, lowest energy structures for the $Ni@Si_{12}$ cluster of C_S and D_{2d} symmetry. The C_S structure, shown in Fig. 1(a), was originally proposed by Singh *et al.*[12] as the lowest energy structure for the $Ni@Si_{12}$ cluster. The C_S isomer can be regarded as a distorted hexagonal prism where one of the Si atoms has elongated bond lengths. The D_{2d} isomer, shown in Fig. 1(b), can be regarded as four joint distorted neighboring pentagons. Slightly higher in energy (0.5 eV above C_S), we find two almost isoenergetic structures [one of which is shown in Fig. 1(c)] of C_1 symmetry. These structures, which apparently correspond to the chairlike structure of Singh *et al.*, are comprised of two parallel distorted pentagons with two apex Si atoms attached on opposite sides of the pentagon planes. The main difference between them is the relative position of the two apex Si atoms.

The D_{2d} isomer was obtained using as an initial geometry an hcp structure with a central Ni atom with first and second neighbors of the central Ni atom. Subsequent frequency calculations have verified that this structure is really stable, corresponding to a minimum of the energy hypersurface. This structure satisfies the isolated rhombus rule (IRR) proposed by Kumar[5] as a criterion of the maximum stability for silicon based "fullerenes" (cages). According to the IRR, in order to minimize the bonding strain, rhombi faces (in this case, square faces) should be placed furthest apart. This originates from the tendency of silicon to create sp^3 bonded structures. The IRR is the analogue of the isolated pentagon rule (IPR) for carbon fullerenes, in which case strain is induced by the existence of pentagons.

In the case of the C_S isomer the structure used as the initial geometry was a hexagonal prism of tight C_{2h} symmetry, as shown in Fig. 1(d). This (hexagonal) structure in itself is significant as it exhibits remarkable stability regardless of the TMA embedded.[27] However, frequency calculations revealed three imaginary values. By performing a continuous cyclic procedure of distorting the structure in accordance to the imaginary frequencies, relaxing the new structure and reevaluating frequencies, in every case we were finally lead to the C_S structure of Fig. 1(a).

The small energy differences between the first few structures in Fig. 1 as well as the procedure mentioned above that

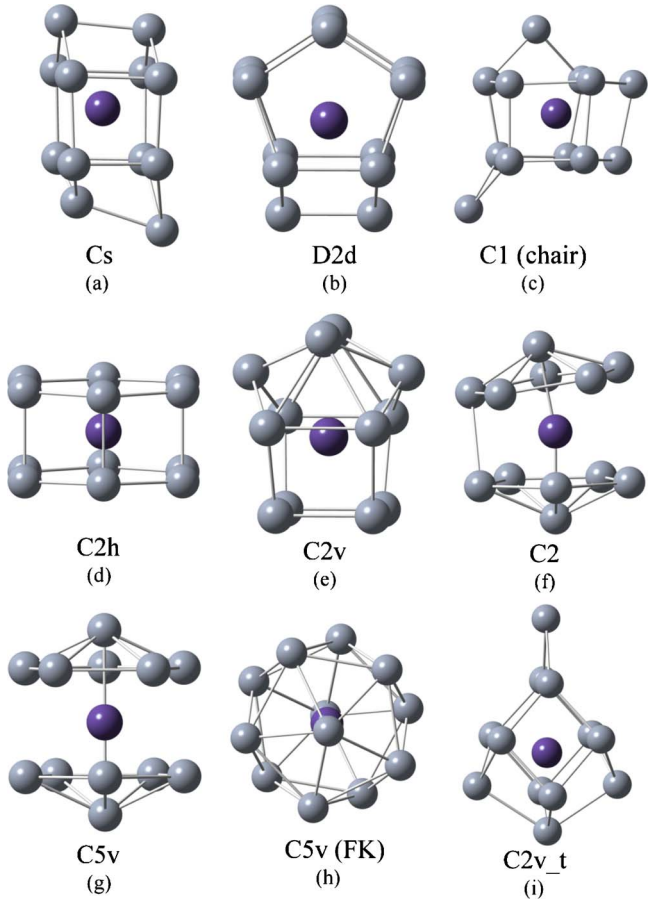

FIG. 1. (Color online) Low energy isomers of the $Ni@Si_{12}$ cluster, ordered from top to bottom by increasing energy (at the B3LYP level). The C_{2v} isomer (i), which has a triplet spin configuration, is placed at the end. Ni-Si bonds have been omitted for clarity. Structures (a) and (b) are isoenergetic at the B3LYP level while the D_{2d} isomer lies much lower at the level of fourth order perturbation theory.

leads to the C_S structure, via a number of intermediate structures, suggests a rather flat potential energy surface, which makes the location of the global minimum difficult. Since the energy difference of the C_S and D_{2d} isomers is only 0.04 eV, which further reduces to about 0.03 eV when zero-point corrections are taken into account, we have performed additional calculations using Møller-Plesset perturbation theory of up to fourth order with the TZVP basis set. This level of fundamental (high order perturbation) and technical (larger basis set) approximations is almost mandatory for such small energy differences. The geometries of the two isomers where reoptimized at the MP2 level of theory and subsequent single-point energy calculations were performed at the MP3 and full MP4 (or MP4SDTQ) level. The results reveal that the energetic ordering of the isomers change at the MP2 and MP4 levels while remaining the same at the Hartree-Fock and MP3 level. In particular, the MP4 results reveal a significant energy difference with the D_{2d} isomer lying 1.3 eV lower than the C_S isomer. The large difference in favor of the D_{2d} isomer is also verified by similar MP4 calculations at the B3LYP geometry. The fluctuations of the energy difference at

various levels of Møller-Plesset perturbation theory is reminiscent of the case of Si_6.[10]

Another low energy isomer, of C_{2v} symmetry [Fig. 1(i)], was obtained from the initial hexagonal geometry with a triplet spin state. It consists of two distorted pentagons [not shown on Fig. 1(i) as they are on the left and right of the structure], neighboring with six distorted rhombi, and caped by a single silicon atom.

The isomer of C_2 symmetry shown in Fig. 1(f) was obtained through distortions of the C_{5v} isomer in Fig. 1(g) following the modes with imaginary frequencies.

The isomer of C_{5v} symmetry shown in Fig. 1(h), known as a Frank-Kasper[28] (FK) structure of 12 neighbors, does not exhibit the stability reported[11] in previous calculations. Frequency calculations reveal modes with imaginary frequencies; thus, this isomer does not correspond to a real minimum. Distortions of this isomer lead to the chair isomer shown in Fig. 1(c). However, its pentagonal prism (two capping Si atoms removed) has been previously used[11] as a building block for the construction of Si nanotubes. The reported stability of these nanotubes is probably not immediately related to the stability of the FK isomer, as has been speculated, but rather is inherent to the nanotube as a whole.

The bonding characteristics of the clusters can be economically and efficiently visualized with a bond length distribution diagram. The comparison of such diagrams for the various isomers could reveal useful qualitative trends related to the observed energetic differences. In Fig. 2 we have plotted the Si-Si bond distribution diagrams for the five energetically lowest isomers that do not exhibit imaginary frequencies, i.e., the isomers denoted as C_S, D_{2d}, Chair, C_{2v} triplet, and C_{2v}, and also for the C_{5v} FK isomer. In the case of C_S and D_{2d}, there is a narrow distribution of the bond lengths with an average value of approximately 2.4 Å, while for the FK isomer the existence of long bonds is evident. We note that long bonds tend to appear as one moves to isomers of increasing energy. The spherical symmetry of the FK isomer

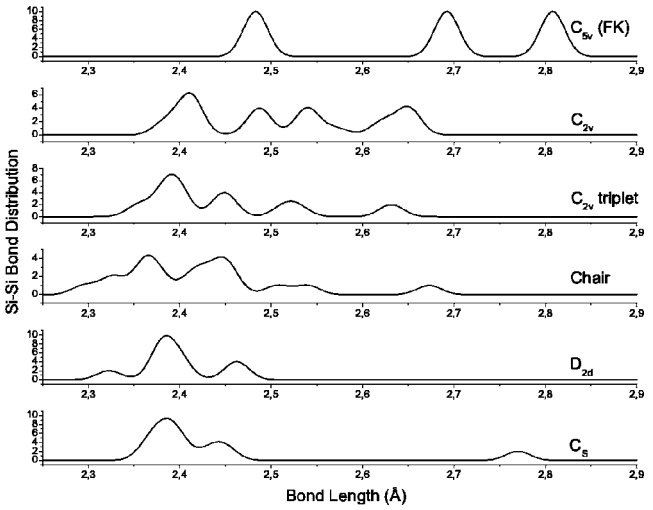

FIG. 2. Si-Si Bond Distribution for the stable isomers C_S, D_{2d}, Chair, C_{2v} triplet, and C_{2v} as well as the C_{5v} FK isomer. The existence of long bonds is evident in the case of the C_{5v} isomer. The ordering of the diagrams is of decreasing energy going from top to bottom.

is not favorable for the Si mesh. This, along with the existence of long bonds, would suggest that the hollow Si C_{5v} cage (i.e., having removed the Ni atom) would benefit (energetically) more than the other two clusters, from the insertion of the Ni atom. Surprisingly enough, a simple examination of the embedding energies reveals that this is not the case.

The ability of a transition metal to stabilize a specific Si cage cluster can be partially quantified by the embedding energy (EE), which is defined as the difference in energy of the transition-metal embedded silicon cluster from the energy of the single Ni atom and of a Si_{12} cluster. Depending on what structure is used for the Si_{12} cluster, there are two distinct definitions, denoted here as EE and EE2. Both of

TABLE I. Energetic properties of the $Ni@Si_{12}$ isomers, total electronic energy (without zero-point energy correction) E, zero-point energy correction ε, Binding energy BE (per atom) HOMO-LUMO gap HL, total energy differences from C_S (without zero-point energy) ΔE, and embedding energies EE, EE2 (see text for difference in definitions). The isomers are ordered by increasing energy. The first three columns include the symmetry of the structures, spin multiplicity, as well as the number of imaginary frequencies obtained by frequency calculations (at the (DFT/B3LYP level). The energy values in parenthesis correspond to the results of full fourth order perturbation theory.

Symmetry	Spin State	Im.	Energy (Ha)	ε (eV)	HL gap (eV)	ΔE from C_s (eV)	BE/atom (eV/atom)	EE (eV)	EE2 (eV)
C_S	s	0	−4981.784 (−4976.779)	0.56	1.55	0.00	3.17	5.43	3.32
D_{2d}	s	0	−4981.783 (−4976.829)	0.55	1.60	0.04	3.17	6.02	3.28
C_1 (chair)	s	0	−4981.765	0.54	1.53	0.51	3.13	5.43	2.82
C_{2h}	s	3	−4981.764	0.52	1.02	0.52	3.13	5.44	2.80
C_{2v}	t	0	−4981.759	0.53	1.20	0.69	3.12	5.44	2.64
C_{2v}	s	0	−4981.755	0.50	1.55	0.78	3.11	5.69	2.54
C_2	s	0	−4981.719	0.46	1.68	1.76	3.03	5.11	1.56
C_{5v}	s	2	−4981.719	0.46	1.67	1.76	3.03	5.13	1.56
C_{5v} (FK)	s	2	−4981.708	0.41	1.16	2.06	3.01	4.49	1.26

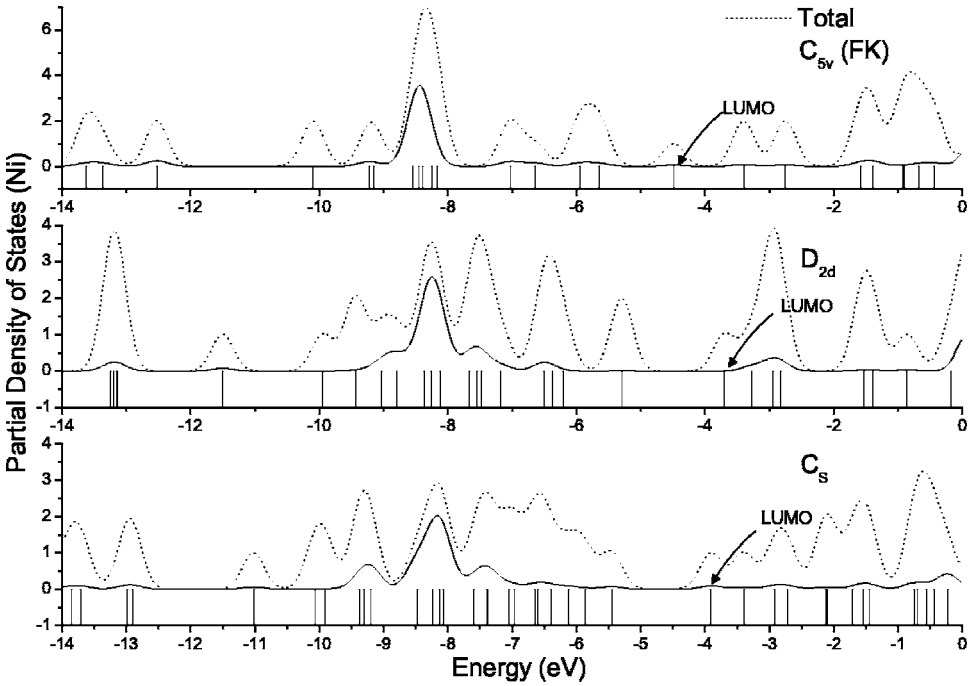

FIG. 3. Energy level diagrams and total and partial density of states diagrams for the two lowest energy isomers (bottom and middle portion of the figure) in comparison with those of the undistorted Frank-Kasper structure (top). The solid lines correspond to contribution to the states from the Ni atom. The dotted lines correspond to the total density of states.

these definitions can be found in current literature. In the case of Ni@Si_{12}, these take the form

$$\mathrm{EE} = [E(\mathrm{Si}_{12})_{hc} + E(\mathrm{Ni})] - E(\mathrm{Ni@Si}_{12}), \tag{1}$$

and

$$\mathrm{EE2} = [E(\mathrm{Si}_{12})_{gs} + E(\mathrm{Ni})] - E(\mathrm{Ni@Si}_{12}), \tag{2}$$

where $(Si_{12})_{gs}$ is the ground state isomer of the Si_{12} cluster[29] and $(Si_{12})_{hc}$ is the hollow cage that remains by removing the Ni atom from the corresponding Ni@Si_{12} isomer. However, it is straightforward to show that the difference in EE2 between two given isomers is equal to the difference in their binding energies (BE),

$$\Delta\mathrm{EE2} = \mathrm{EE2}_{isom1} - \mathrm{EE2}_{isom2} = \mathrm{BE}_{isom1} - \mathrm{BE}_{isom2} = \Delta\mathrm{BE}, \tag{3}$$

and as a result, an EE2 energy diagram follows exactly that of a BE diagram, obviously at a different energy scale. The first definition gives an insight on the stabilizing effects of the Ni atom for the specific structure, while the second definition provides a means of comparing the relative stability of each Ni@Si_{12} isomer. Here we present calculations based on both definitions. Both definitions have merits and drawbacks. Perhaps the first definition is more relevant to the present discussion.

The values of the embedding energies in Table I present large variation from one structure to the other. Four of the isomers have an EE value of around 5.4 eV. The highest EE found is that of the D_{2d} isomer, which suggests a significant stabilizing effect of the embedded Ni atom. The high BE as well as the quite large highest occupied molecular orbital-lowest unoccupied molecular orbital (HOMO-LUMO) gap of this isomer is indicative of its stability. Since the C_{5v} FK isomer has the lowest EE value, this structure benefits energetically the least by the insertion of a Ni atom in the hollow FK Si cage. This is actually the opposite of what would be expected on the basis of our earlier discussion. Since the C_{5v} structure is very unfavorable for the pure Si_{12} cluster, one would expect that this cluster would benefit the most.

As a means to facilitate the comparison of the energy levels between different isomers, we have plotted in Fig. 3 the total density of state (DOS) and the partial density of state (PDOS) (nickel contribution) for the two energetically lowest isomers as well as the FK isomer. These curves were generated from the eigenvalues of the ground state B3LYP/TZVP calculations with a suitable Gaussian broadening. The PDOS of the embedded Ni atom (solid line) appear quite similar for all clusters, with a major peak (and perhaps a few more, secondary peaks) centered on the energy region of −9.5 to −7.5 eV. The main contribution to these peaks originates from the *d* orbitals of the nickel atom, with the overall Ni contribution ranging from 51% to 78%. For the case of C_S (mostly) and D_{2d} (lesser) clusters, we can see a significant level splitting of Ni *d* orbitals, which can be attributed to a nonisotropic field induced by the Si network. The effect is not present in the case of C_{5v} isomer, which has a more "spherical" shape and higher symmetry. In this energy region, there are Ni-related states (for the cases of the C_S and D_{2d} isomers) which exhibit a strong antibonding character. On the other hand, for the case of the C_{5v} FK isomer, all of the nickel related states in the specific energy region are bonding. This differentiation can be considered as a result of the loose binding of the silicon network (long bonds), which allows (through charge density redistribution) the formation of Si-Ni bonding states.

In Fig. 4 we display the Ni contribution to the DOS as well as the PDOS of the Ni related *d* states and the projected DOS for each Ni 3*d* atomic orbital.

In Fig. 5 we show the COOP diagrams for the same three isomers. The dotted lines correspond to the overlap of every Ni atomic orbital (AO) with every Si AO. The solid lines

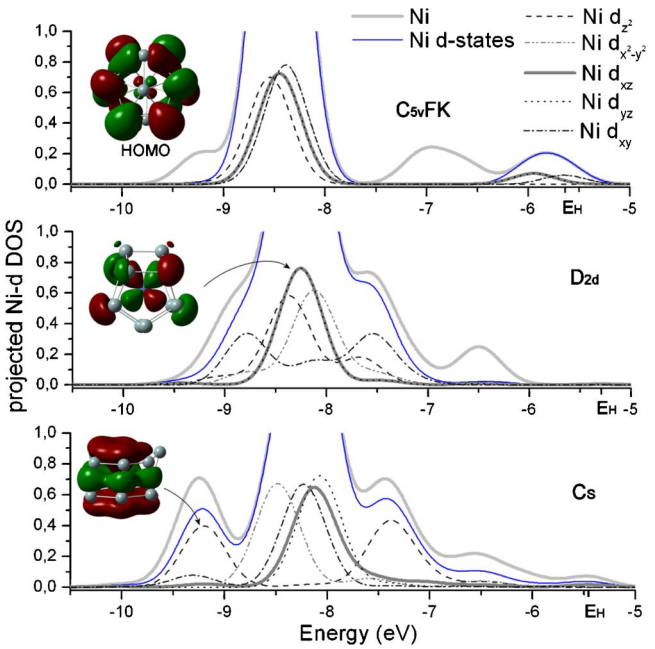

FIG. 4. (Color online) Projected Ni-d density of states diagrams for the two lowest energy isomers in comparison with those of the (undistorted, unstable) Frank-Kasper structure. The energy level of the HOMO is denoted by E_H.

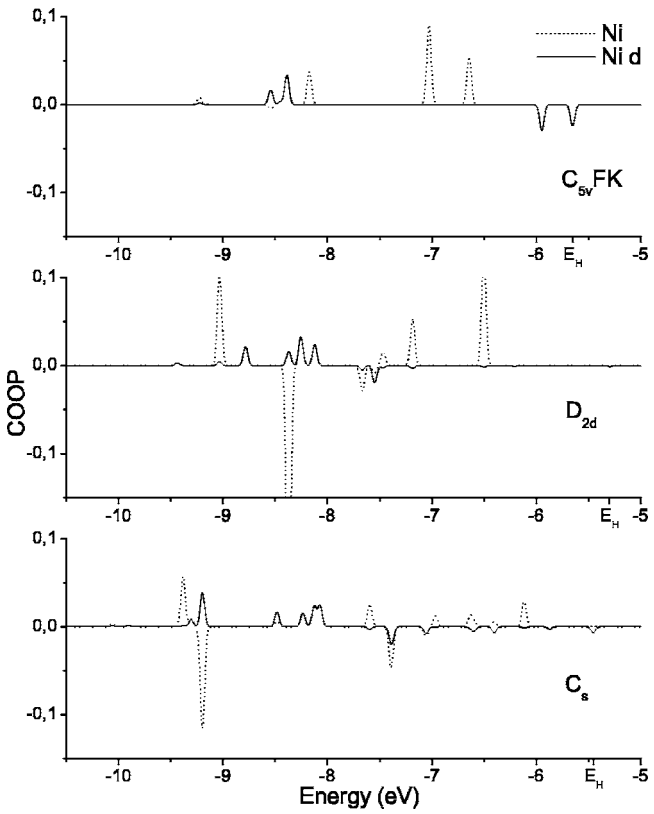

FIG. 5. Crystal Orbital overlap population (COOP) diagrams. The dotted lines correspond to the overlap of the Ni AOs with those of every Si. The solid lines are similar as the dotted lines; except that only Ni-d states are included. The energy level of the HOMO is denoted by E_H.

correspond to the overlap of the Ni-d AOs with every Si AO.

The crystal field splitting of the Ni 3d levels is clearly shown in Fig. 4. This level splitting is more noticeable in the case of the C_S isomer. In this case, the Ni d state DOS has three peaks, of which the main peak is comprised of Ni d_{xy}, d_{yz}, d_{xz}, and $d_{x^2-y^2}$ states, while the two peaks at the sides correspond to Ni-d_{z^2} related states, one being bonding (at −9.2 eV) and the other antibonding (at −7.3 eV). The inset image in Fig. 4 for C_S corresponds to this Ni-d_{z^2} bonding state. This state gives the largest positive peak in the corresponding COOP diagram for C_S. In the case of the D_{2d} isomer, the central peak consists of Ni d_{yz}, d_{xz}, d_{z^2}, and $d_{x^2-y^2}$ states, while the (less noticeable compared to the C_S case) side peaks correspond to the d_{xy}-dominated Ni states. The bonding level is located at −8.8 eV and the antibonding at −7.5 eV. In this case, the central peak has a significant contribution from the Ni d_{xz} and d_{yz} states, which remain degenerate as expected due to the symmetry planes on which they lie. The molecular orbitals corresponding to these states are shown in the inset image in Fig. 4 for D_{2d}. The only case in which we have clearly antibonding contribution, although marginal, from the Ni d states near the Fermi level is for the C_{5v} FK isomer; see, for instance, the HOMO in the inset of Fig. 4 for C_{5v} FK. Also, from Fig. 4 the almost complete lack of crystal field splitting is evident for the case of the C_{5v} FK isomer.

There were no trends found by our attempts to examine as to whether e_g (d_{z^2} and $d_{x^2-y^2}$) or t_{2g} (d_{xy}, d_{yz}, and d_{xz}) symmetric orbitals are filled first as a general trend in every isomer. As can be seen in all the PDOS diagrams, the contribution of the Ni-related states to the DOS declines as the energy approaches the Fermi level. However, the (small) proportion of the Ni contribution is not the same for all isomers. In particular, the percentage of the Ni contribution to the HOMO in the case of the C_{5v} FK isomer is about 6%, and around 7% for the C_S isomer. In both cases, at the HOMO the Ni states overlap with the Si states is antibonding (negative overlap). In the case of the D_{2d} isomer there is no contribution (zero) from the Ni to the HOMO. As a result, the HOMO has a Si sp character. Furthermore, the Ni sp states in the energy region from −7.5 eV up to the Fermi level are mainly bonding, while the Ni d states are nonbonding (or slightly antibonding), as we can infer from the COOP diagrams. These results regarding Ni are in agreement with the conclusions of Mpourmpakis *et al.*,[30] who found that in going from left to right of the 3d series of the transition metals, the characters of the HOMO (and LUMO) changes from metal d-like to silicon sp-like. The strong silicon sp-character of the HOMO in the case of the C_{5v} FK isomer can be seen in the first inset image in Fig. 4.

In the COOP diagram for each of the isomers, a clear separation of bonding-antibonding Ni d states appears. As noted earlier, in each case, antibonding Ni related states exist in the energy region of −9.5 to −7.5 eV. From the Ni d state COOP curves (solid lines), we see that these antibonding states are not Ni-d related states (but rather, s and p type), and probably do not depend on the number of d electrons of the embedded transition metal. The reasoning behind this is that TM-d electrons contribute to the bonding after any other s or p state (with the exception in some cases of the 4s state).

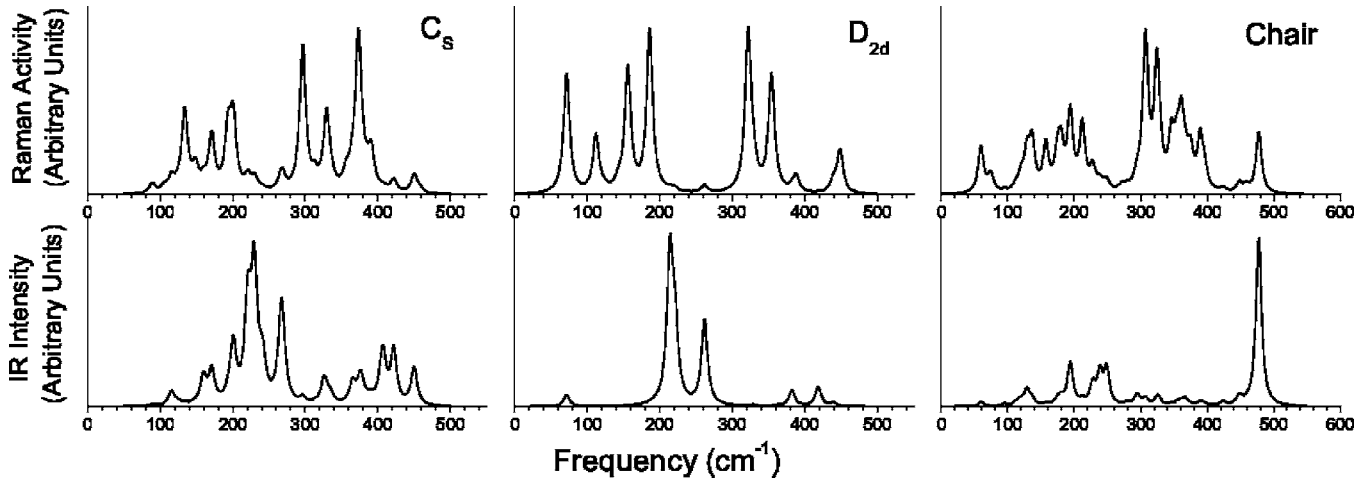

FIG. 6. Raman and IR spectrum (obtained by a suitable Gaussian broadening) of the three energetically lowest isomers of $Ni@Si_{12}$, denoted as C_S, D_{2d}, and Chair. Calculations were performed at the DFT/B3LYP level.

In order to facilitate the experimental characterization of the $Ni@Si_{12}$ cluster, we have calculated Raman activities and IR intensities for the three energetically lowest isomers (Fig. 6). The frequencies with the highest activities and intensities (Raman and IR) for the C_S and D_{2d} isomers are also given explicitly in Table II.

In all cases, the contribution of the Ni atom to the higher frequencies of the Raman and IR spectra is either nonexistent

TABLE II. Selected dominant Raman and IR (infrared) frequencies, together with the corresponding Raman activities A and IR intensities I, for the two energetically lowest isomers, of C_S and D_{2d} symmetry.

C_S			D_{2d}		
ω (cm^{-1})	Raman A (Å^4/amu)	IR I (km/mole)	ω (cm^{-1})	Raman A (Å^4/amu)	IR I (km/mole)
133.6	27	0	71.5	27	2
133.8	8	0	71.5	27	2
148.4	10	0	112.0	13	0
159.5	4	2	112.0	13	0
170.8	24	3	155.9	56	0
193.4	25	0	185.9	54	0
200.6	30	5	186.5	20	0
220.6	6	8	214.0	1	26
228.8	2	7	214.0	1	26
230.9	3	4	221.0	1	24
241.0	1	3	261.6	2	15
266.6	6	6	261.6	2	15
269.3	3	2	321.8	72	0
296.5	62	0	329.2	4	0
325.7	2	2	329.2	4	0
329.5	31	1	353.9	47	0
365.2	7	2	355.6	6	0
373.4	64	0	382.3	1	3
376.5	3	2	382.3	1	3
391.1	16	0	418.6	0	3
405.5	0	2	418.6	0	3
408.0	1	2	439.5	5	1
421.8	5	4	448.7	19	0
450.0	8	3	—	—	—
133.6	27	0	—	—	—

TABLE III. Energetic properties of the $Ni@Si_{12}$ isomers, vertical ionization potential IP, vertical electron affinity EA, chemical potential μ, and chemical hardness η. The isomers are characterized by their symmetry group.

Sym	IP (eV)	EA (eV)	μ (eV)	η (eV)	μ/η
C_S	6.69	2.54	−4.62	2.07	−2.23
D_{2d}	6.57	1.92	−4.24	2.33	−1.82
C_1 (chair)	6.70	2.59	−4.64	2.06	−2.26
C_{2h}	5.90	2.31	−4.10	1.80	−2.28
$C_{2v}t$	6.59	2.67	−4.63	1.96	−2.37
C_{2v}	6.89	2.64	−4.76	2.13	−2.24
C_2	7.05	2.69	−4.87	2.18	−2.23
C_{5v}	7.31	2.69	−5.00	2.31	−2.16
C_{5v} (FK)	7.16	3.05	−5.11	2.05	−2.49

or negligible. Above a specific (to each isomer) threshold, the spectra are dominated by the Si cage vibrations. In the case of the C_S isomer, this threshold is at 335 cm^{-1} and for the D_{2d} isomer at 261 cm^{-1}. Obviously, this is related to the larger mass of the Ni atom, which results in low values of frequency for the modes dominated by Ni. Furthermore, the vibrations of the Ni atom contribute mainly to the IR intensities while the vibrations of the Si cage contribute mostly to the Raman activities.

The D_{2d} isomer has two doubly degenerate modes of the IR spectrum with frequencies 214 and 261 cm^{-1} as well as one at 221 cm^{-1}, each of which is dominated by the vibrations of the Ni atom. The breathing mode of the Si cage gives a peak in the Raman spectrum at 322 cm^{-1}, while a very similar to the breathing mode is found at 354 cm^{-1}. The Raman peak at 449 cm^{-1} corresponds to the (nearly horizontal) vibrations of the two Si atoms on the bottom and their symmetry equivalent on the top (movement transverse to the page). For the C_S isomer, the peak in the Raman spectrum at 373 cm^{-1} can be considered as the breathing mode (not all silicon atoms contribute the same to this mode). The peaks at 296 and 329 cm^{-1} correspond to a twisting motion of the silicon atoms on the hexagons' planes. By comparing the spectra of the C_S and D_{2d} isomers, it becomes obvious that for the identification of the two isomers both Raman and IR spectroscopy may be necessary. The chairlike isomer can easily be identified by the intense peak in the IR spectrum at 477 cm^{-1}, which corresponds to the vibrations of an apex Si atom.

A property of interest[31,32] of TMA-doped Si clusters, or composite materials from these clusters, could be their ability to act as charge sources to other macroscopic or microscopic bodies. For this purpose we have calculated the chemical potential (μ) and chemical hardness (η) of these structures. It has been shown[31,32] that a guiding principle to predict the occurrence of an easier charge transfer between two chemical systems, 1 and 2, is a large difference in μ together with low values of η_1 and η_2. Therefore, the quantities of interest are the chemical potential and chemical hardness along with the ionization potential and electron affinity. These quantities are evaluated as follows.

The chemical potential and chemical hardness (absolute hardness) are the first and second derivatives of the electronic energy of the system with respect to the number of electrons at a constant external potential.[31] Evaluation of the chemical potential and hardness is performed by a finite difference approximation resulting in the following relations:

$$\mu = \frac{IP + EA}{2}, \quad \eta = \frac{IP - EA}{2}, \tag{4}$$

where the ionization potential IP and the electron affinity EA are evaluated from the energies of the $N-1$, N, and $N+1$ electron systems at the neutral cluster geometry,

$$\mathrm{IP} = E_{N-1} - E_N, \quad \mathrm{EA} = E_N - E_{N+1}. \tag{5}$$

Although the ionization potential can be accurately predicted, the evaluation of the electron affinities can exhibit problems. When the experimental electron affinity is negative, direct evaluation of the hardness using Eq. (4) is intrinsically problematic. This is due to an artificial binding of the excess electron caused by the finite basis set. When using larger basis sets that include diffuse functions, the electron is able to leave the system; thus, the calculated EA becomes near zero and the chemical hardness approaches IP/2. In such cases alternative methods of evaluating the chemical hardness have been recently suggested.[33] In our case, for such clearly positive values of the electron affinity of the magnitude presented here, the method of Eq. (5) that we have used gives the most accurate results.

In Table III, we have summarized the results of our calculations for the vertical ionization potentials and electron affinities as well as the chemical potentials and hardness of each isomer. It should be noted that these values are calculated at the ground state geometry of the neutral clusters. As a result, direct comparison with experiment (or other calculations) should be carried out with caution (especially for

EA), to avoid confusion with adiabatic electron affinities or vertical detachment energies (these quantities involve structural relaxation of the charged cluster). A benchmark calculation of the vertical ionization potential for the ground state isomer of the Si_{12} cluster[29] gives a value of 7.39 eV, which is in excellent agreement with the experimentally obtained[34] range of 7.17–7.46 eV.

Clusters with a high ability to accept an electron accompanied by a low chemical hardness are among those with a large $|\mu/\eta|$ ratio ($|\mu/\eta|>3$ as suggested by Miyazaki *et al.*[32]). As can be seen in Table III, the most promising of the $Ni@Si_{12}$ isomers to act as a charge-transfer-type acceptor to other macroscopic substances would have been the C_{5v} Frank-Kasper structure (if it was stable). However (even in this hypothetical case), the rather high value of the hardness suggests that it would not have been suitable.

CONCLUSIONS

In summary, using density functional theory and employing the B3LYP functional we have identified a new ground state structure of the $Ni@Si_{12}$ cluster of D_{2d} symmetry, which at the level of forth order perturbation theory is energetically lower by 1.3 eV compared to the previously known lowest lying isomer of C_S symmetry, derived from a hexagonal structural motif. At the DFT/B3LYP level of theory, the two structures are practically isoenergetic with a difference of 0.04 eV (0.03 eV when including zero-point corrections to the energy). The new D_{2d} structure, with a cubic structural motif, satisfies the IRR stability criterion proposed by Kumar. The energetic ordering of the C_S and D_{2d} isomers seems to depend strongly on the level of correlation included in the calculations. In particular, the C_S isomer appears to be energetically lower in the Hartree-Fock and MP3, level of theory, while at the MP4 level of theory, the D_{2d} structure is found to be significantly lower in energy. Contrary to earlier reports, the C_{5v}, derived from an icosahedral structural motif, is unstable (exhibits imaginary frequencies) and lies significantly higher in energy. To facilitate possible future experimental characterization of the clusters, we provide IR and Raman spectra for the two lowest isomers. Our calculations of vertical ionization potentials, electron affinities, chemical potentials, and chemical hardness reveal that these structures cannot be expected to act efficiently as possible charge-transfer-type acceptors to other substances.

ACKNOWLEDGMENTS

We thank the University of Patras/Research Committee and particularly the basic research program "K. KARATHEODORI 2003" and the European Social Fund (ESF), Operational Program for Educational and Vocational Training II (EPEAEK II), and particularly the program PYTHAGORAS, for funding the above work.

*E-mail address: zdetsis@upatras.gr

[1] S. N. Khanna, B. K. Rao, and P. Jena, Phys. Rev. Lett. **89**, 016803 (2002).
[2] V. Kumar, Eur. Phys. J. D **24**, 227 (2003).
[3] J. Lu and S. Nagase, Phys. Rev. Lett. **90**, 115506 (2003).
[4] G. Mpourmpakis, G. E. Froudakis, A. N. Andriotis, and M. Menon, Phys. Rev. B **68**, 125407 (2003).
[5] V. Kumar, Comput. Mater. Sci. **30**, 260 (2004).
[6] R. T. Tung, J. M. Gibson, and J. M. Poate, Phys. Rev. Lett. **50**, 429 (1983).
[7] P. J. van den Hoek, W. Ravenek, and E. J. Baerends, Phys. Rev. Lett. **60**, 1743 (1988).
[8] S. M. Beck, J. Chem. Phys. **87**, 4233 (1987); **90**, 6306 (1989).
[9] H. Hiura, T. Miyazaki, and T. Kanayama, Phys. Rev. Lett. **86**, 1733 (2001).
[10] A. D. Zdetsis, Phys. Rev. A **64**, 023202 (2001); A. D. Zdetsis, Computing Letters **1**, 337 (2005).
[11] M. Menon, A. Andriotis, and G. Froudakis, Nano Lett. **2**, 301 (2002); A. Andriotis, G. Mpourmpakis, G. Froudakis, and M. Menon, New J. Phys. **4**, 78 (2002).
[12] A. K. Singh, T. M. Briere, V. Kumar, and Y. Kawazoe, Phys. Rev. Lett. **91**, 146802 (2003).
[13] A. D. Becke, Phys. Rev. A **38**, 3098 (1988); J. P. Perdew, Phys. Rev. B **33**, 8822 (1986).
[14] A. Schäfer, H. Horn, and R. Ahlrichs, J. Chem. Phys. **97**, 2571 (1992).
[15] K. Eichkorn, O. Treutler, H. Öhm, M. Häser, and R. Ahlrichs, Chem. Phys. Lett. **240**, 283 (1995).
[16] P. J. Stephens, F. J. Devlin, C. F. Chabalowski, and M. J. Frisch, J. Phys. Chem. **98**, 11623 (1994).
[17] C. S. Garoufalis, A. D. Zdetsis, and S. Grimme, Phys. Rev. Lett. **87**, 276402 (2001); C. S. Garoufalis and A. D. Zdetsis, Phys. Chem. Chem. Phys. **8**, 808 (2006).
[18] A. Schäfer, C. Huber, and R. Ahlrichs, J. Chem. Phys. **100**, 5829 (1994).
[19] TURBOMOLE Version 5.6, Universitat Karlsruhe, 2000.
[20] M. V. Arnim and R. Ahlrichs, J. Chem. Phys. **111**, 9183 (1999).
[21] GAUSSIAN 03, Revision C.02, Gaussian, Inc., Wallingford, CT, 2004.
[22] C. Peng, P. Y. Ayala, H. B. Schlegel, and M. J. Frisch, J. Comput. Chem. **17**, 49 (1996).
[23] K. Jackson, M. R. Pederson, D. Porezag, Z. Hajnal, and T. Frauenheim, Phys. Rev. B **55**, 2549 (1997); E. C. Honea, A. Ogura, C. A. Murray, Krishnan Raghavachari, W. O. Sprenger, M. F. Jarrold, and W. L. Brown, Nature **366**, 42 (1993), and references therein.
[24] *Vibrational Intensities in Infrared and Raman Spectroscopy*, edited by W. B. Person and G. Zerbi (Elsevier, New York, 1982).
[25] C. Møller and M. S. Plesset, Phys. Rev. **46**, 618 (1934).
[26] T. Hughbanks and R. Hoffmann, J. Am. Chem. Soc. **105**, 3528 (1983).
[27] P. Sen and L. Mitas, Phys. Rev. B **68**, 155404 (2003).
[28] F. C. Frank and J. S. Kasper, Acta Crystallogr. **11**, 184 (1958).
[29] X. L. Zhu, X. C. Zeng, and Y. A. Lei, J. Chem. Phys. **120**, 8985 (2004).

[30] G. Mpourmpakis, G. E. Froudakis, A. N. Andriotis, and M. Menon, J. Chem. Phys. **119**, 7498 (2003).
[31] R. G. Parr and W. Yang, *Density-Functional Theory of Atoms and Molecules* (Oxford University Press, New York, 1989) 74, 95 regarding hardness, and 91–92 regarding charge transfer.
[32] T. Miyazaki, H. Hiura, and T. Kanayama, Eur. Phys. J. D **24**, 241 (2003).
[33] D. J. Tozer and F. de Proft, J. Phys. Chem. A **109**, 8923 (2005).
[34] K. Fuke, K. Tsukamoto, F. Misaizu, and M. Sanekata, J. Chem. Phys. **99**, 10 (1993).